

Distribution Agreement

In presenting this thesis as a partial fulfillment of the requirements for a degree from Emory University, I hereby grant to Emory University and its agents the non-exclusive license to archive, make accessible, and display my thesis in whole or in part in all forms of media, now or hereafter now, including display on the World Wide Web. I understand that I may select some access restrictions as part of the online submission of this thesis. I retain all ownership rights to the copyright of the thesis. I also retain the right to use in future works (such as articles or books) all or part of this thesis.

Zhuoting Xie

04/08/2025

Video-based quantitative analysis of orofacial movements in a Parkinson's Disease Mouse

Model

by

Zhuoting Xie

Dieter Jaeger, PhD
Adviser

Biology

Dieter Jaeger, PhD
Adviser

Gordon Berman, PhD
Committee Member

Adriana Galvan, PhD
Committee Member

2025

Video-based quantitative analysis of orofacial movements in a Parkinson's Disease Mouse

Model

by

Zhuoting Xie

Dieter Jaeger, PhD

Adviser

An abstract of
a thesis submitted to the Faculty of Emory College of Arts and Sciences
of Emory University in partial fulfillment
of the requirements of the degree of
Bachelor of Science with Honors

Biology

2025

Abstract

Video-based quantitative analysis of orofacial movements in a Parkinson's Disease Mouse Model

By Zhuoting Xie

Parkinson's disease (PD) manifests with both motor and non-motor symptoms, including facial hypomimia and olfactory dysfunction. To characterize these orofacial features, we conducted a longitudinal, video-based analysis of facial and nose movements in MitoPark mice—an established transgenic model of PD—during a head-fixed, bi-directional water-reaching task. Using synchronized dual-view video recordings, we quantified facial motion energy (FME) for selected face regions and tracked nose movement. Trials were categorized by behavioral outcome and reward direction, and both amplitude and bout metrics of movement were analyzed across age. A total of 4 MitoPark and 3 control mice were tested across multiple weeks spanning early to late ages during Parkinsonism symptom progression. Our analysis revealed that FME captured subtle but progressive changes in facial activity in MitoPark mice. In particular, motion in the Whisker region decreased with age, consistent with facial hypomimia, while activity in the Eye and Upper Nose regions increased, possibly reflecting dysregulated or stress-related movements. Movement bout analysis showed increased bout occurrence with age, which may reflect impaired ability to execute sustained facial movements. In contrast, nose movement traces revealed lateralized response biases toward sensory cues in some individual mice (regardless of genotype), while a general decline in nose movement amplitude was observed across MitoPark mice over time. This decline, along with reduced pre- and post-reward nose movement bouts, may indicate olfactory-related impairments such as diminished sniffing, aligning with early-stage PD pathology. Overall, this study provides a detailed, time-resolved characterization of orofacial movement changes in MitoPark mice that contributes to a more comprehensive non-motor and motor symptom profile of the MitoPark model and further supporting its relevance as a preclinical model of Parkinson's disease.

Video-based quantitative analysis of orofacial movements in a Parkinson's Disease Mouse

Model

by

Zhuoting Xie

Dieter Jaeger, PhD

Adviser

A thesis submitted to the Faculty of Emory College of Arts and Sciences
of Emory University in partial fulfillment
of the requirements of the degree of
Bachelor of Science with Honors

Biology

2025

Acknowledgements

I would like to sincerely thank my advisor, Dr. Dieter Jaeger, for his continuous support and mentorship—both in research and in shaping my career path. His insights have deeply enriched my understanding of neuroscience and fueled my passion for the field. I am also grateful to the current and past members of the Jaeger Lab for their valuable suggestions and support throughout my research journey. In particular, I would like to thank Elijah Lapeza for his tremendous help in animal training and data collection, Dr. Su Li for assisting with the behavioral experiment setup, Lisa Meyer-Baese for providing the original script used in motion energy calculation, and Indeara Martinez for training the first cohort of animal. I am especially thankful to Dr. Aurélie Pala for her meticulous mentorship and continued guidance, which first introduced me to neuroscience research and has been instrumental in shaping my scientific development.

I gratefully acknowledge the support from the Parkinson's Foundation Summer Student Fellowships Program (Identifier: 1298292) and the Udall Center grant (Identifier: 1P50NS123103), which made this work possible.

I would also like to thank my committee members, Dr. Gordon Berman and Dr. Adriana Galvan, for their time, valuable feedback, and insightful contributions to my project. Particularly, I would like to thank Dr. Berman for his two engaging classes, which sparked my interest in computational neuroscience. In addition, I would like to thank the Udall Histology Core and its director, Dr. Galvan, for assistance with mouse brain histology.

Finally, I would like to express my heartfelt thanks to Dr. Bayona Vásquez, who has mentored me since my first days at Oxford College of Emory and has supported me throughout my entire college career.

Table of Contents

Introduction	1
Methods	5
Results	13
Discussion	25
References	31
Supplementary Figures	36

Chapter 1: Introduction

1.1 Parkinson's Disease and Orofacial Deficits

Parkinson's disease (PD) is a neurodegenerative disorder characterized by progressive motor and nonmotor symptoms that predominantly affect the aging community. The pathology of PD is marked by degeneration of dopaminergic neurons (DA), particularly in the substantia nigra pars compacta, leading to characteristic motor symptoms such as tremor, bradykinesia, and rigidity¹. In addition to well-established motor impairments, PD also presents a wide range of non-motor symptoms, which may precede motor deficits and significantly impact quality of life, including cognitive decline, sleep disturbances, autonomic dysfunction, mood disorders, olfactory deficits, and orofacial symptoms such as hypomimia. Hypomimia, a symptom characterized by reduced spontaneous (e.g. blinking), emotional, and intentional facial expressions due to deteriorated coordination in facial musculature, which primarily reflects basal ganglia dysfunction². The experience of hypomimia, also commonly known as the masked face, is strongly associated with social rejection and depression in PD patients, which can contribute to diminished quality of life for both the patients and their caretakers³.

The control of facial movement is governed by complex interactions between the basal ganglia, cerebral cortex, and cerebellum, which together modulate downstream motor pathways (Fig. 1). Beyond its role in thalamo-cortical regulation, the basal ganglia influence brainstem motor centers such as the red nucleus (RN), a critical hub for coordinating facial and head movements. Output from the entopeduncular nucleus (EN), one of the main outputs from the Basal Ganglia, reaches the RN both directly and indirectly through the zona incerta (ZI) and fields of Forel (FF), with additional modulation from the subthalamic nucleus (STN). These pathways converge within the RN, which also receives input from nuclei within the cerebellum, allowing integration

of basal ganglia and cerebellar signals. The RN then projects to the facial nucleus (FN) and upper cervical spinal cord, linking upstream regulatory centers to motor execution⁴. This circuitry provides a pathway through which basal ganglia dysfunction due to dopamine depletion in PD can lead to deficits in voluntary and automatic facial movements by disrupting coordinated muscle control across the network. In addition to facial movement impairments, deficits in orofacial sensorimotor function and olfactory sensitivity have been observed in both human patients and mouse models of Parkinson's disease. Studies report that PD patients often struggle with odor detection and discrimination⁵, as well as impaired sniffing ability⁶. Similarly, PD mouse models have demonstrated reduced olfactory sensitivity⁷, highlighting the broader disruption of orofacial and sensory processing associated with dopaminergic dysfunction. Hypomimia and olfactory dysfunction⁸ have been increasingly recognized as potential biomarkers for prodromal PD diagnosis, as they manifest early in PD^{8,9}. In this case, it is essential to recapitulate hypomimia symptoms observed in humans using more accessible animal models, such as mice models, so that we can capture detailed motor features and a timeline of symptom progression. More importantly, we may associate orofacial movement with neural imaging data to dissect the neural underpinnings of alterations in orofacial movement during PD development.

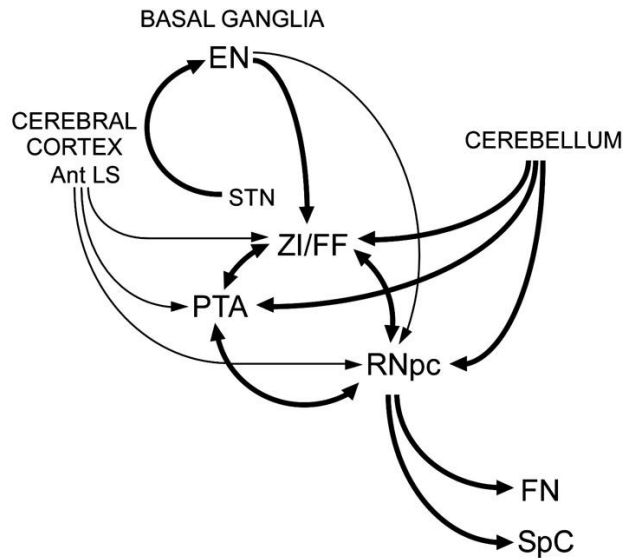


Fig. 1: Schematic of neural pathways involved in the control of facial musculature by the basal ganglia and cerebellum. Figure adapted from Pong et al.,⁴. Abbreviations: EN, entopeduncular nucleus; STN, subthalamic nucleus; ZI/FF, zona incerta/field of Forel; PTA, pretectal area; RNpc, parvocellular red nucleus; FN, fastigial nucleus; SpC, spinal cord; Ant LS, anterior limbic system.

1.2 MitoPark mouse model of PD

In this project, we used the transgenic MitoPark mouse model of Parkinson's disease (PD) to examine age-dependent changes in facial and nose movements. MitoPark mice develop progressive parkinsonian symptoms due to targeted inactivation of the mitochondrial transcription factor A (Tfam) specifically in dopamine transporter (DAT)-expressing neurons, leading to mitochondrial dysfunction and gradual degeneration of the dopaminergic system¹⁰. As shown in Fig. 2¹¹, detectable loss of tyrosine hydroxylase (TH)-positive neurons and striatal fibers, accompanied by a modest decline in locomotor activity, typically emerges around 12–14 weeks. More pronounced motor deficits—such as bradykinesia and reduced spontaneous

movement—begin to manifest by 20 weeks and progressively worsen beyond 30 weeks. In addition to motor deficits, MitoPark mice also display a range of non-motor symptoms including olfactory discrimination impairments, anxiety-like behaviors, and cognitive decline¹²—closely paralleling the multifaceted pathology of human PD. These features make MitoPark mice a well-suited model for studying both motor and non-motor aspects of disease progression.

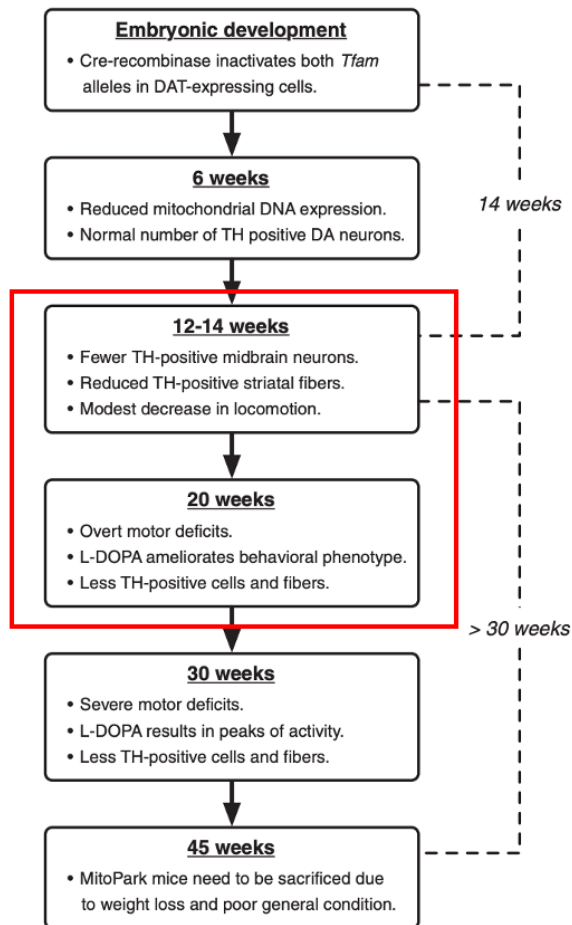


Fig. 2: Schematic of disease progression in the MitoPark mouse model of Parkinson's disease.

The red box outlines the typical experimental window used in this study, during which behavioral training begins around 8 weeks of age and video-based recordings continue through approximately week 25. Figure adapted from Ekstrand et al¹¹.

1.3 Objective and hypotheses

Previous rodent studies have established the role of the dopaminergic pathway in regulating orofacial movements and the association between dopamine deficiency in the striatum and orofacial dysfunction^{13,14}. Additionally, Evidence from Tomiyama et al.¹⁵ demonstrates that stimulation of D1-like dopamine receptors in mice induces distinct orofacial behaviors such as vertical tongue protrusions or vibrissae movement, while antagonism of these receptors suppresses these responses. These findings suggest that dopamine depletion in PD could lead to altered orofacial movement topography. This evidence, along with olfactory dysfunction seen in MitoPark mouse model, led us to two preliminary hypotheses that MitoPark mice will show 1) a decrease in orofacial movement evidenced by reduced motion energy, and 2) reduced nose movement in response to reward as a sign of Parkinsonia symptom manifestation compared to their littermate controls as they age. We will extract and quantify the essential features of mice's facial movements and track changes in nose movement with videos recorded from head-fixed mice during a bilateral directional reward reaching task.

Chapter 2: Materials and Methods

2.1 Animals and Water Restriction Protocol

A total of 4 MitoPark (1 female and 3 males) and 3 littermate control mice (3 females) were used in this study, spanning ages from 8 to 35 weeks (with MitoPark mice sacrificed before week 30). Mice were housed under a reverse light cycle (12 h light / 12 h dark) with running wheel in their home cages as enrichment. All training and behavioral recordings were conducted during the dark phase. Prior to headpost surgery, mice were handled for at least one day. Following surgery,

animals were habituated to the head-fixation setup for a minimum of 5 days before training commenced to minimize potential stress. During this period, they were placed under continuous water restriction, and body weight was closely monitored to ensure it remained above 80% of baseline (weight before water restriction). After the training phase, mice underwent EMG implantation surgery (for a separate project), after which they were switched to ad libitum 2.5% citric acid water.

2.2 Reaching Task and Behavioral Recording

Mice were trained on a bilateral directional reaching task in which they were required to reach toward the water reward (0.1% saccharine + 0.4% Kool-Aid) using the limb on the same side as the reward spout. Each trial began with a paw resting period (≤ 5 s), followed by a 2 s baseline (no reach), a pseudorandom delay (0.75–1.25 s), and then a go cue—either a brief auditory tone (1s,) or a white light flash (0.3 s). The reward was then randomly delivered through either the right or left spout, followed by a 5 s response window, a 5 s consumption period, and a 2 s inter-trial interval (see Fig. 3). A successful trial was defined as a correct-side reach during the response window. Failure trials included: (1) no response (no contact with either spout), signaled by a failure tone (1s) or a 1 s 5 Hz blue light, (2) wrong-side reaches, and (3) early reaches (contact during the baseline or delay periods). Only successful and no-response trials were considered in the orofacial movement analysis.

To monitor and record behavioral events, the experimental setup included: 1) A head-fixation station with a 3D-printed tube angled at 45°, featuring two metal paw-rest bars, 2) A gravity-based water delivery system providing precise and consistent dispensation of small water volumes, with two spouts placed bilaterally in front of the animal, 3) A stimulus delivery system for presenting either light or sound cues. The first cohort ($n = 3$, 2 MitoPark and 1 Control)

received light cues via an LED panel, and the second cohort ($n = 4$, 2 MitoPark and 2 Control) received auditory tones via a speaker embedded in the setup (since light cue skewed pupil signals which we wanted to measure initially), 4) Capacitive touch sensors on the spouts and paw bars to detect contact and reaching attempts. 5) A dual-camera high-speed video recording system (Basler a2A1920-160um), with one bottom-view camera for nose/mouse tracking and one side-view camera for limb/facial tracking. Videos from both cameras were recorded at 100 frames per second (FPS) with image size 1216×900 pixels in .mp4 format. LED lighting was used to illuminate the scene without interfering with animal behavior. Recordings were conducted inside a light-tight enclosure.

To control and synchronize the experiment, the Bpod State Machine r2 (Sanworks) was used. Bpod handled task flow and sent digital TTL pulses (square wave signals) to external devices, including the LED panel, speaker, and solenoid valves for water delivery. Additionally, Bpod triggered frame-by-frame video capture by sending 100 Hz TTL pulses to the camera system, enabling precise synchronization of behavioral events with video data. All input (e.g., sensor activations) and output signals (e.g., reward delivery, cue presentation, video triggers) were timestamped, allowing cross-modal alignment for post-hoc analysis.

Animals were trained for up to 14 consecutive days to achieve $\geq 50\%$ success rates (out of >100 trials/session). Control mice typically learned the task in fewer sessions than MitoPark mice. Some MitoPark mice developed strong side biases, consistently reaching only to one spout. Only sessions after task acquisition were used for facial and nose movement analysis.

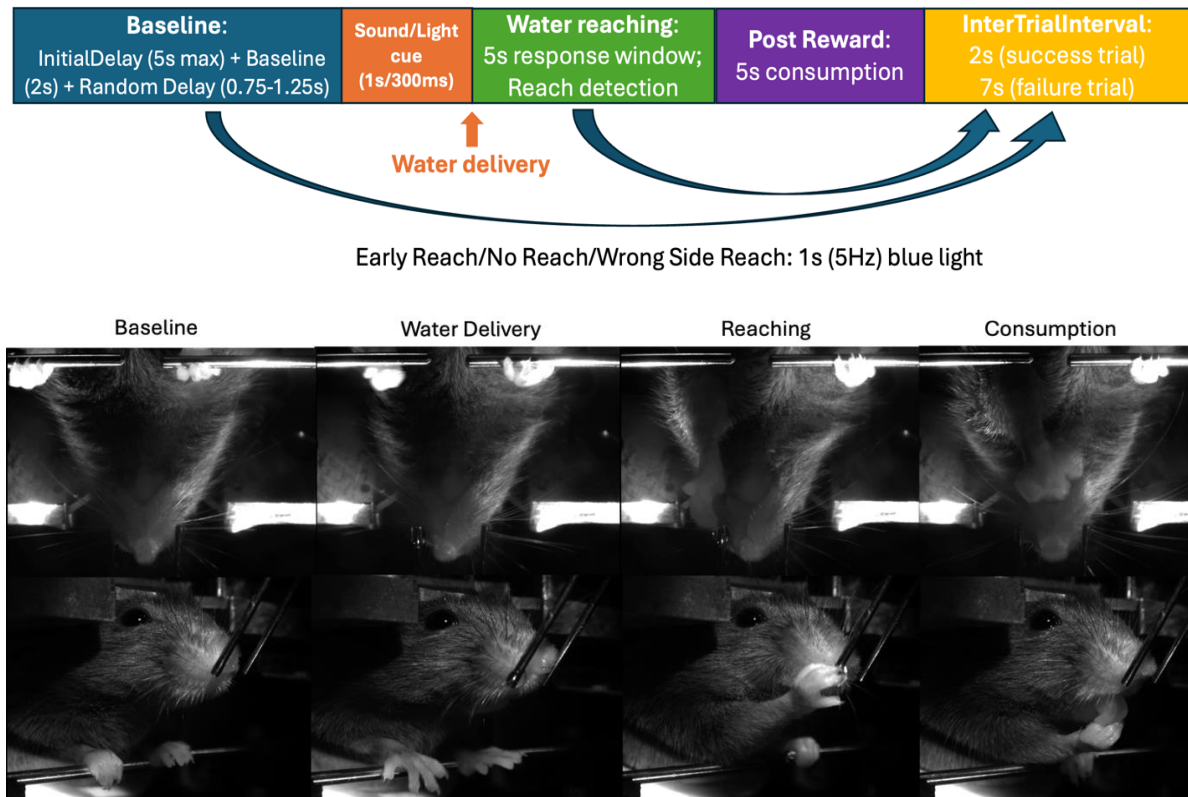


Fig. 3: Top: Schematic showing the trial structure of the reaching task. Bottom: sample success reaching trial and reaching setup recorded for bottom and side views.

2.3 Analysis of data

2.3.1 Immunochemistry and Reaching performance Characterization

The reaching performance taken from the Bpod output was first quantified to assess overall motor function changes. The probability of each trial type (NoReach, Reach, EarlyReach, and WrongSideReach) and the average reaction time for mice to touch the correct spouts after reward dispensation was calculated for sessions from each week of age for both MitoPark ($n = 4$) and Control mice ($n = 3$). At the end of all experiments, all MitoParks along with control mice were perfused, and $50\text{-}\mu\text{m}$ sections were cut and processed for TH immunostaining (Hamamatsu) in the striatum and substantia nigra.

2.3.2 Facial motion energy (FME) calculation

FME was defined as the average pixel-wise absolute difference between consecutive frames¹⁶, calculated within manually positioned, fixed-size regions of interest (ROIs) on the mouse's face (ROI defined as in Fig 4). To reduce variability across sessions due to changes in lighting conditions, each frame was first histogram-matched to a reference image (an example frame selected from a recording with balanced lightening) using the built-in MATLAB function *imhistmatch*. The FME at each time point t was computed as:

$$\text{FME}_t = \frac{1}{N} \sum_{i=1}^N |\text{imhistmatch}(I_t(i), I_{\text{ref}}) - \text{imhistmatch}(I_{t-1}(i), I_{\text{ref}})| \quad (1)$$

where N is the total number of pixels in an ROI, $I_t(i)$ is the intensity of i^{th} pixel at frame t , and I_{ref} is an reference image used for histogram equalization across all frames for all recordings to account of lightening intensity change across different sessions. The raw FME traces were then smoothed with a third-order 1D median filter (*medfilt1*).

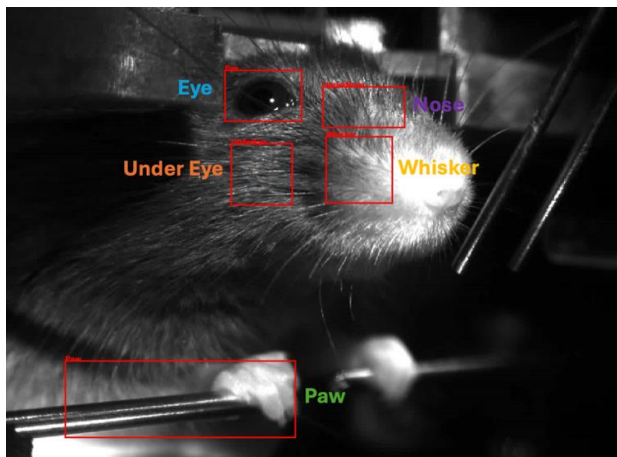


Fig. 4: Face ROIs where FME is calculated. The ROIs were manually placed on each video at roughly the same facial locations to account for variabilities of mouse's head position in the setup.

2.2.3 Nose movement analysis

To ensure precise quantification of nose movement, we used DeepLabCut 3.0 (DLC)¹⁷, a deep learning-based markerless pose estimation toolbox, to track nose position from the bottom-view camera recordings after cropping the videos to 450×450 . A nose-tracking model was trained on 180 labeled frames across 9 videos, and ResNet-50 backbone architecture along with the multi-animal tracking workflow. A total of eight keypoints were placed along the rim of the nose to capture its outline. For each frame, nose position was defined as the centroid of these eight points, provided that at least six of the trackers met quality control criteria. Specifically, only keypoints with a DLC confidence score > 0.6 and no abrupt displacements (defined as first derivatives exceeding the 95th percentile of frame-to-frame displacement within a session) were included for centroid calculation. Frames that did not meet this criterion were assigned NaN values. These missing values were then interpolated using the shape-preserving piecewise cubic interpolation method, *pchip (interp1)*. The resulting position trace was further smoothed using a 2nd-order low-pass Butterworth filter with a cutoff frequency of 10 Hz to suppress high-frequency tracking jitters (see Fig. 5, right panel for example of preprocessing steps). The X (horizontal) and Y (vertical) position traces were analyzed separately. For each trace, the distribution of nose positions was centered such that the most frequent position (distribution peak) was set to zero. After centering, negative values in the horizontal (X) trace indicate leftward movement and positive values indicate rightward movement. Similarly, negative values in the vertical (Y) trace reflect upward movement, while positive values indicate downward movement relative to the centered nose position.

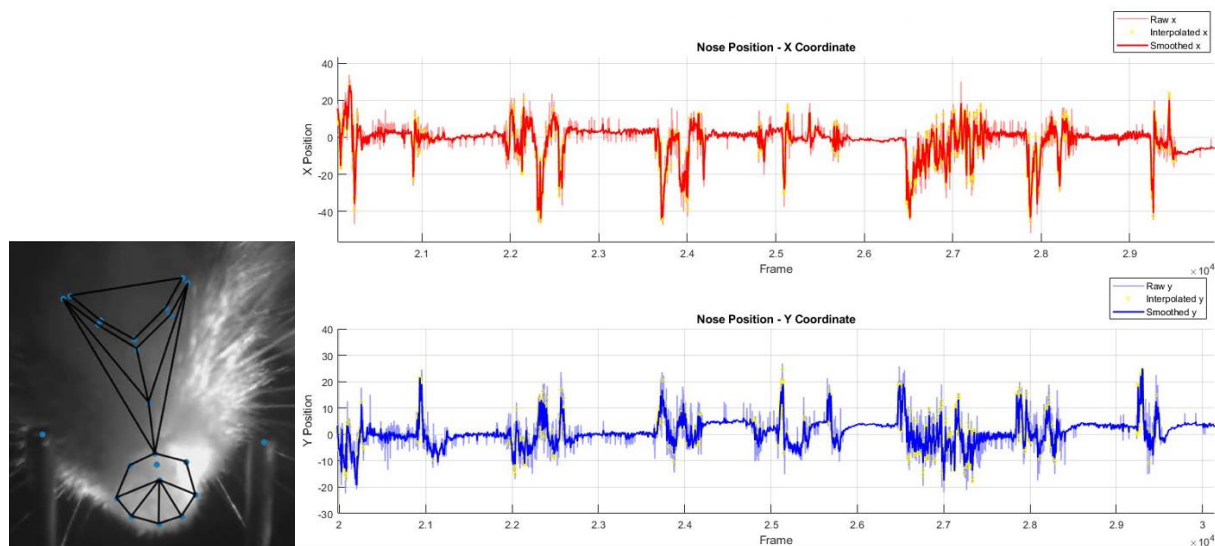


Fig. 5: Left: DLC Nose tracking sample. Right: Nose position pre-processing example.

2.2.4 Quantification and statistical analysis of behavioral data

Both FME and Nose movement traces were computed within a time window of ± 3 seconds centered around reward delivery. This window captures both spontaneous and reward-driven facial dynamics, such as reaching and water consumption in successful trials, and differential movement patterns in no-response trials. Only trials with perfect synchronization between video and Bpod pulses (i.e., total frame count equal to the number of TTL timestamps) were included for analysis. Across all $n = 7$ mice, a total of 4,258 no-response and 6,815 reach trials were used for FME analysis, while 4,149 no-response and 7,234 reach trials were used for nose movement analysis. For group comparisons, trials were divided into four groups: 1) all trials from Control mice ($n = 3$), 2) MitoPark ($\leq W17$): sessions before or during Week 17, 3) MitoPark (W18–W20), and 4) MitoPark ($\geq W21$): sessions during or after Week 21. Within each group, data were further subdivided by trial type. For FME analysis, trials were categorized into NoReach and Reach (Left vs. Right). For nose movement analysis, both NoReach and Reach trials were both split

based on reward side, since directionality is crucial for understanding lateral nose movement.

Table 1 shows the number of trials for each data group.

	Nose Movement				FME		
	NoReachL	NoReachR	ReachL	ReachR	NoReach	ReachL	ReachR
Control	74	132	2607	2480	167	2474	2352
\leq W17	241	299	825	455	419	787	310
W18 - W20	852	725	574	182	1577	574	186
\geq W21	955	871	82	29	2095	98	34

Table 1: Number of trials for partitions of data between Control and different age periods of MitoPark mice as well as different trial types.

To assess changes in movement patterns, we computed the average signal as the area under the curve (AUC) per frame over the 6-second analysis window for each trial, using the absolute value of the nose position trace. To further characterize facial and nose dynamics, movement bout duration was quantified from both FME and absolute nose position traces. A movement bout was defined as a continuous period of activity above a predefined threshold lasting at least 0.1 seconds. For FME, signals were first baseline-corrected by subtracting the minimum value within each trial, then rescaled such that the mean signal across all trials in a session was normalized to 1 for each ROI. A fixed threshold of 0.5 was then applied uniformly across all ROIs. For absolute horizontal nose position, the trace was similarly baseline-corrected, and a fixed threshold of 10 pixels was used to identify bouts. This standardized thresholding approach enabled consistent comparison of movement patterns across sessions and groups. Note that movement bouts were analyzed separately before and after reward presence within time windows. For nose movement, both the peak amplitude and its directionality (i.e., positive or negative displacement) were quantified for each trial.

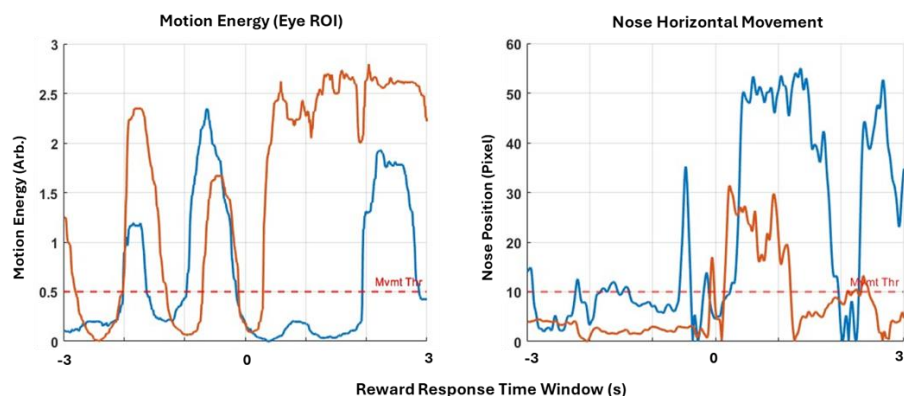


Fig. 6: Method for Movement bout length identification for FME and nose movement.

2.4 Statistical Test

All statistical significance tests reported in this study used the Wilcoxon Rank Sum Test (U-test) to compare group medians due to non-parametric distributions, and all p-values were adjusted with Bonferroni correction for multiple statistical tests. To quantify effect sizes, the two-sample difference in medians was computed along with bootstrapped 95% confidence intervals (NumBootstraps = 1000). All data analysis and statistical testing were performed in MATLAB 2024b.

Chapter 3: Results

3.1 Immunochemistry and Reaching performance characterization

To confirm dopamine depletion in the MitoPark mice, we examined TH staining in the striatum and substantia nigra of control and MitoPark mice. In control animals, intense TH immunoreactivity was observed in the striatum and SN, indicating robust dopaminergic projections and cell bodies. In contrast, MitoPark mice exhibited a marked reduction in TH

staining intensity in the striatum (Fig. 6a), along with a loss of TH-positive fibers and soma in the SN, particularly the substantia nigra pars compacta (SNpc) region (Fig. 6b).

For reaching performance, the correct-side reach rate for MitoPark started to drop significantly around week 17, while the control stays consistently the same (Fig. 7). The reaching response time showed similar pattern where we observed progressively slower response toward reward as the MitoPark age, comparing to control mice' stable response time (Fig. 7).

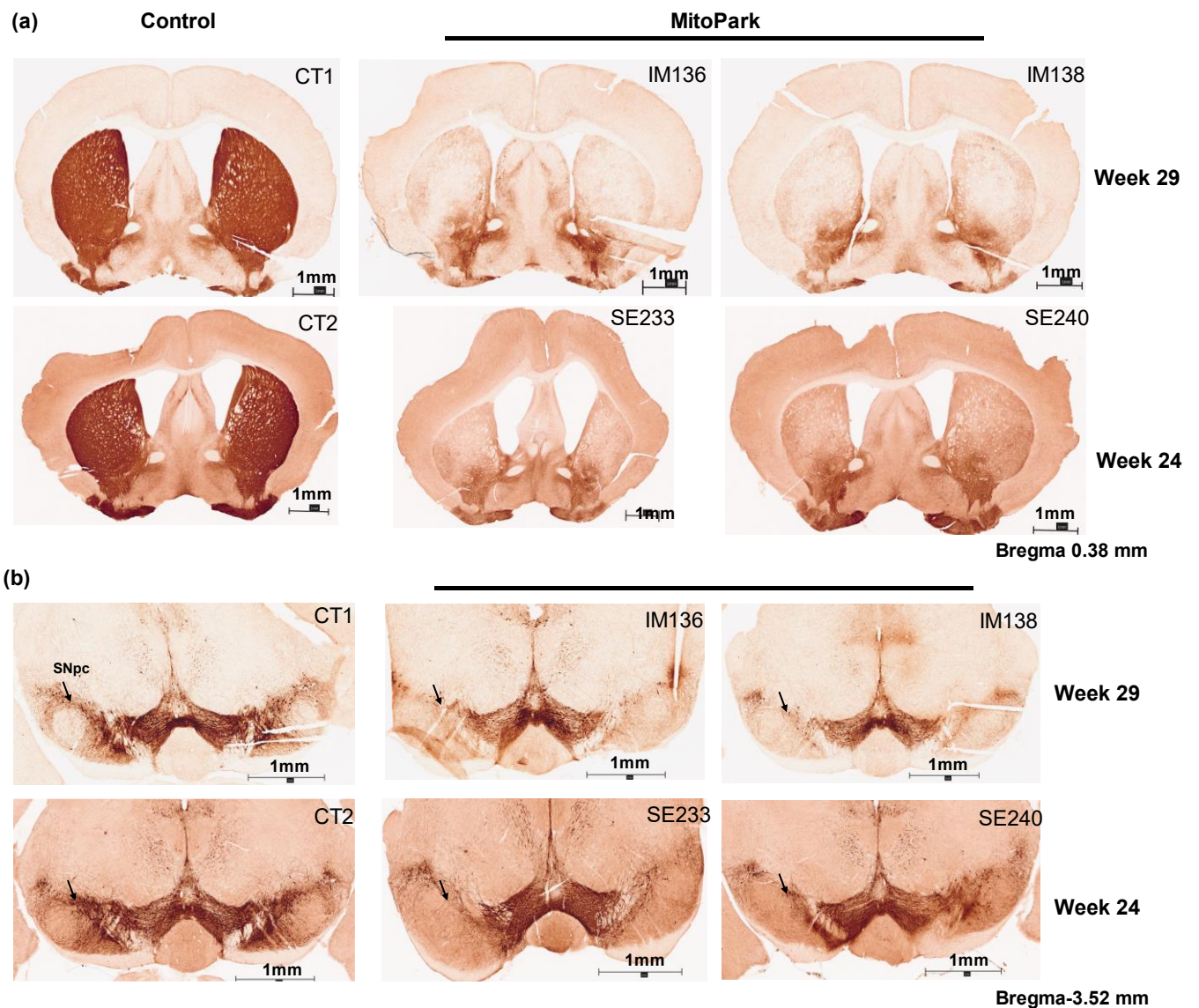


Fig. 6: Representative coronal sections of control and MitoPark mouse brains showing TH immunoreactivity in the dorsal striatum (a) and substantia nigra pars compacta (SNpc) (b). Bar =1000 μ m. Bregma values were based on Paxinos's Mouse Brain Atlas.

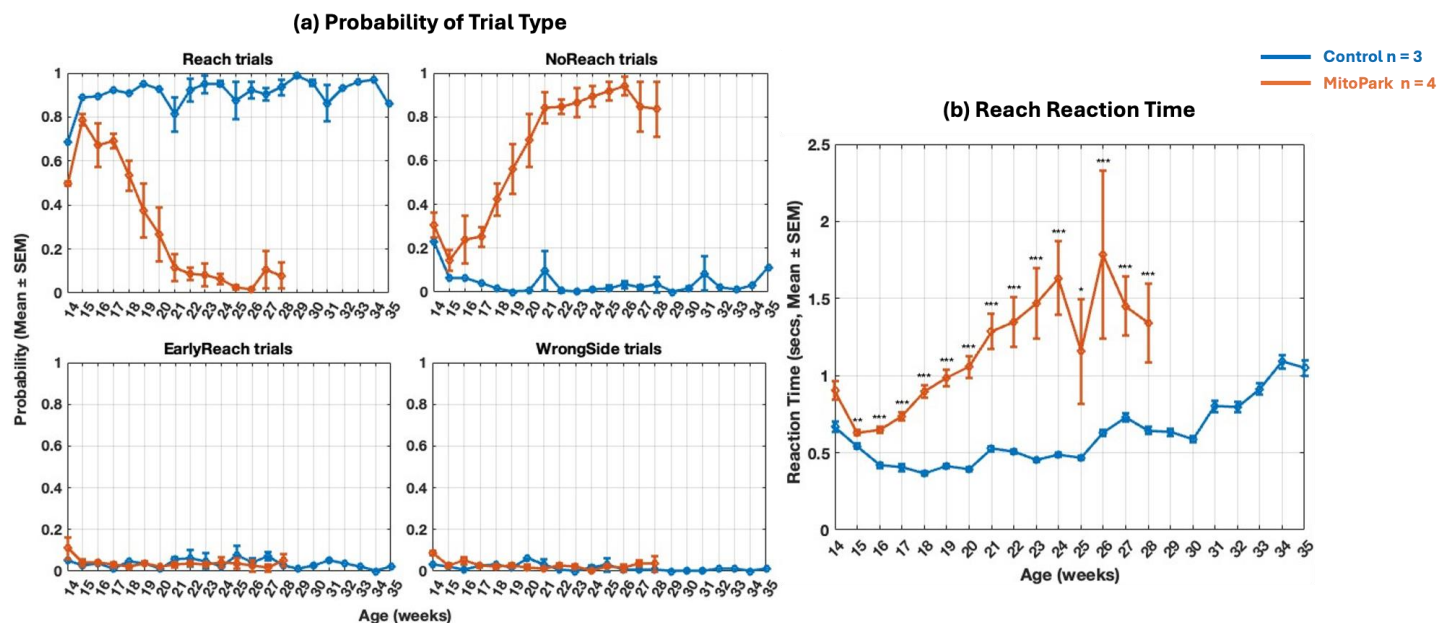


Fig. 7: (a) Probability of each trial type and (b) reward-reaching reaction time between MitoPark and Control mice across age. Asterisks indicate statistical significance between groups at each time point ($p < 0.05$: *; $p < 0.01$: **; $p < 0.001$: ***).

3.2 FME and Nose Movement Traces Aligned to Reward Response Time Window

To characterize how facial movements evolve during behavioral responses, we first examined individual FME traces aligned to the reward response window. As shown in Fig. 8, FME increased markedly after reward delivery, capturing the expected facial dynamics associated with licking and water consumption. The FME signal also reflected more subtle movements such as blinking and whisker twitching and revealed trial-type-specific motion patterns. For example, NoReach trials exhibited consistently lower FME amplitudes, while successful Reach trials showed strong post-reward motion bursts. Fig. 9 displays FME traces averaged over all trials

from representative Control and MitoPark sessions, demonstrating the temporal alignment between the rise in FME and the reaction time to reward contact. Notably, in the MitoPark session from a later age, the amplitude of FME—especially during Reach trials—was diminished, suggesting a progressive reduction in facial movement. Based on observed ROI dynamics, three regions were selected for further analysis: Eye, Whisker, and Upper Nose, to capture squinting and subtle twitches on the face.

Nose position analysis revealed characteristic movement patterns across trial phases. During the baseline period, we observed small oscillatory fluctuations around zero, likely reflecting spontaneous sniffing behavior. Upon go-cue onset, we observed a rapid lateral shift in nose position toward the rewarded side, initiating the directional reach, followed by a quick return toward the center during the consumption period (Fig. 10). Notably, some animals exhibited biased movement strategies, where the nose initially shifted to one side regardless of the reward location, then corrected orientation based on reward side. For example, in Fig. 11, the mouse initially moved its nose leftward after the go cue, but subsequently redirected rightward to reach the correct spout, resulting in a longer reaction time for rightward trials—consistent with a left-side preference. When comparing averaged nose trajectories across sessions, MitoPark mice in advanced weeks displayed reduced horizontal movement amplitudes in both Reach and NoReach trials, suggesting a general movement decline toward sensory cues. For further analysis, only horizontal movement traces were considered.

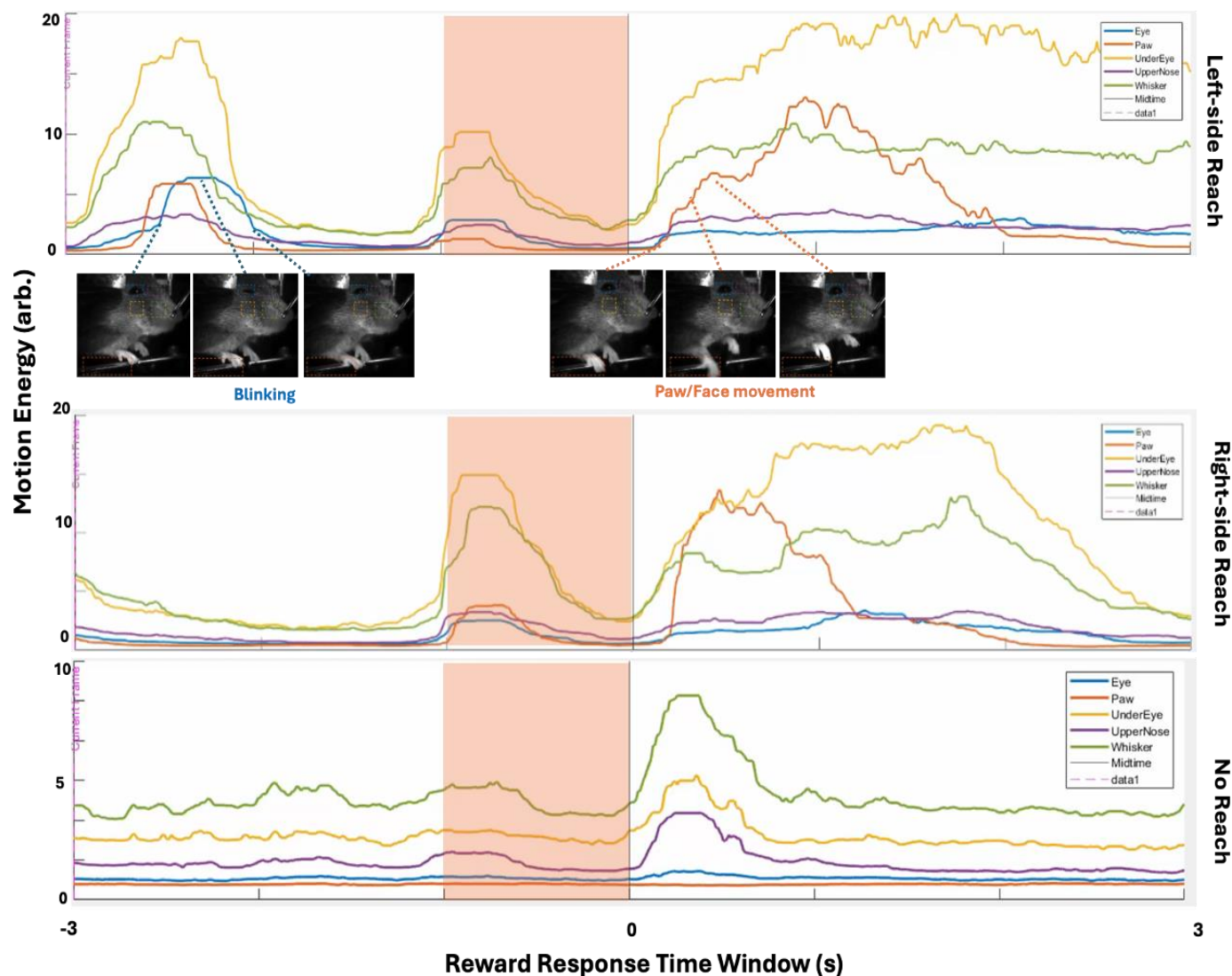


Fig. 8: Example facial motion energy (FME) traces from a single Control mouse session, aligned to the reward response window across different trial types. The shaded red region indicates the window starting from go cue onset (1s duration sound cue in these trials). Sample frames here illustrated specific facial movements such as blinking, paw, and facial movement.

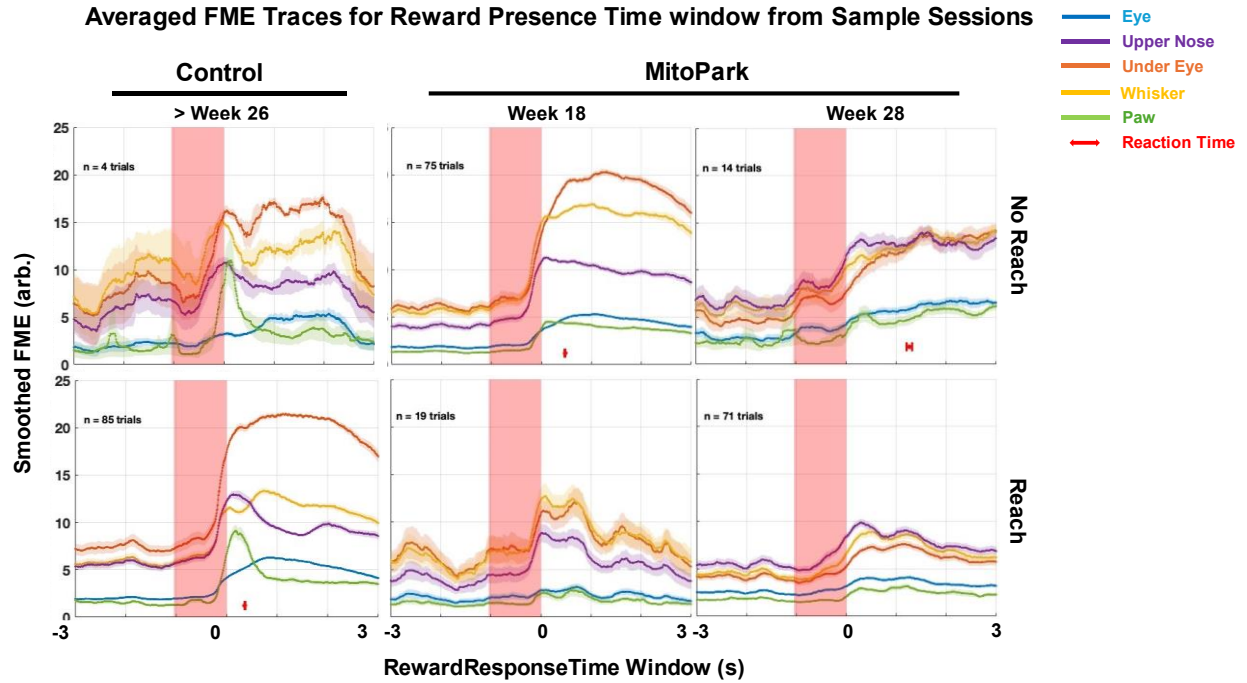


Fig. 9: Averaged FME traces across trials for different trial types from one Control and one MitoPark mouse session. Lines and the shaded regions represent mean FME and the standard error mean (SEM) respectively across trials within one session. The red error bar marks the mean and SEM of reaction times for reward reaching.

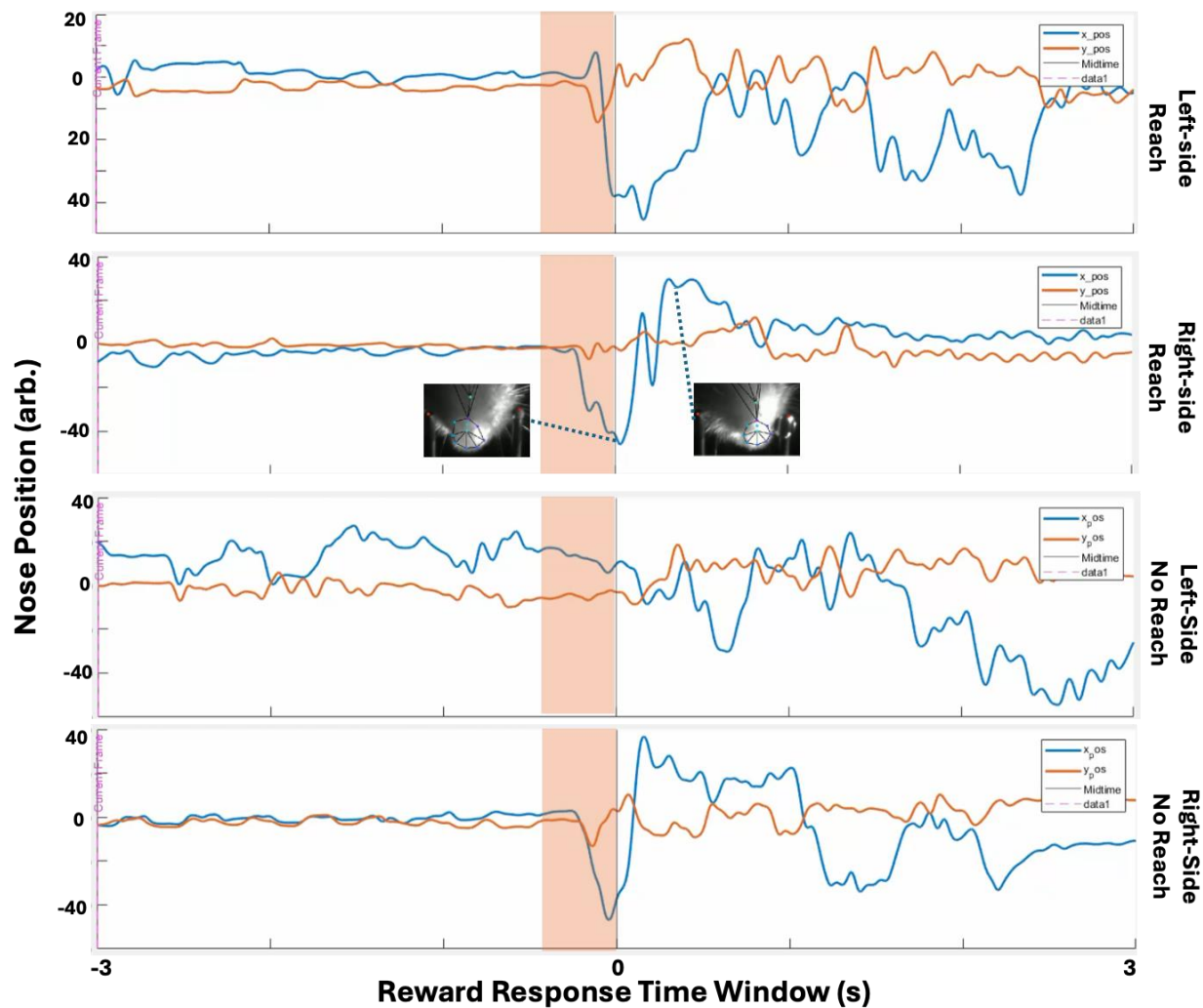


Fig. 10: Example nose movement trajectories during reward response time window from a Control mouse session. Plots show horizontal (blue) and vertical (orange) nose position for representative Reach and NoReach trials. The red-shaded region indicates the go cue window (light cue onset, 0.3 s). Insets show tracked nose positions aligned with directional movement.

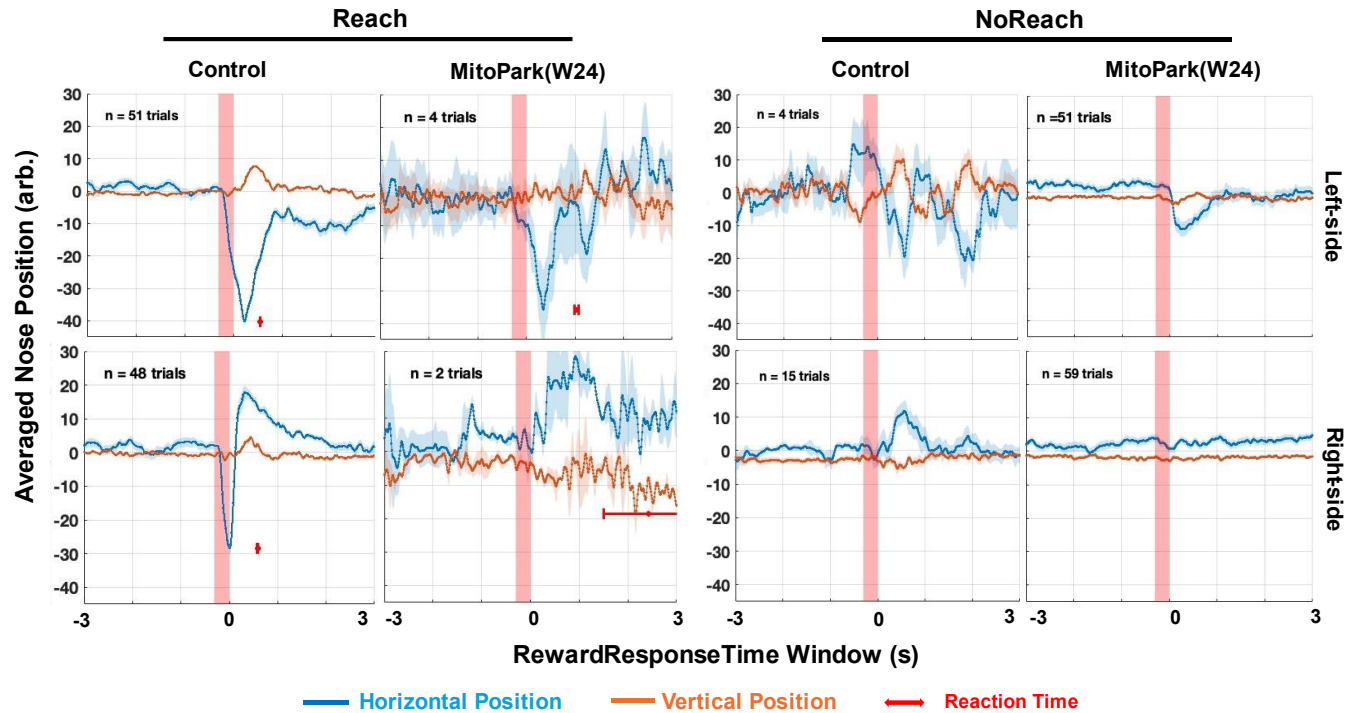


Fig. 11: Averaged nose position traces during reward response window for Reach vs. NoReach trials across sample sessions. Traces reflect horizontal and vertical movement relative to center. Red-shaded region marks cue onset. Red arrows mark average reaction time where available. Reduced movement amplitudes are evident in advanced-week MitoPark sessions.

3.3 Characterization for FME and Nose Movement over Time

As expected, reaching trials elicited greater facial motion energy (FME) than NoReach trials across all ROIs ($p < 0.001$ for all within-group comparisons of NoReach vs. ReachL/ReachR). In the Whisker ROI, average FME decreased significantly in late-stage MitoPark mice ($\geq W21$) compared to both Controls and early-stage mice ($\leq W17$) during NoReach ($p < 0.001$) and ReachR ($p < 0.001$) trials, reflecting progressive motor impairment. Conversely, FME in the Eye and UpperNose ROIs increased with age in MitoPark mice across all trial types (Eye: $p < 0.001$ for all trial types; UpperNose: $p < 0.001$ for NoReach and ReachL), suggesting compensatory or

dysregulated facial activity with disease progression (Fig. 12a). Movement bout length (Fig. 12b) showed a mild but consistent increase before reward delivery in late-stage MitoPark mice during ReachL trials across both Eye and UpperNose ROIs ($p < 0.05$, $\leq W17$ vs. $\geq W21$), potentially indicating prolonged or less refined facial motion. After reward, the Eye ROIs in late-stage mice exhibited shorter bouts in right-side reach trials (Eye: $p < 0.001$), with a broader distribution suggesting a shift toward more fragmented movement. Post-reward changes in UpperNose ROI were not statistically assessed due to bimodal distributions and limited data.

Nose movement analyses (Fig. 13) revealed reduced average lateral nose position during NoReachL and NoReachR trials in $\geq W21$ MitoPark mice compared to both Controls and $\leq W17$ mice ($p < 0.001$), indicating diminished voluntary lateral movement (Fig. 13a). This decline was mirrored in peak displacement amplitudes (Fig. 13b), with significantly reduced leftward and rightward extremes during NoReach and ReachR trials ($p < 0.001$, $\leq W17$ vs. $\geq W21$). In contrast, ReachL trials showed increased absolute leftward peak amplitudes in $\geq W21$ mice ($p < 0.001$), hinting at a directional movement bias. Movement bout length (Fig. 13c) remained mostly stable, though post-reward NoReach trials showed modest reductions in bout length in late-stage mice ($p < 0.001$, $\leq W17$ vs. $\geq W21$). Full statistical outcomes and effect sizes are detailed in the Fig. 12 and Fig. 13 captions.

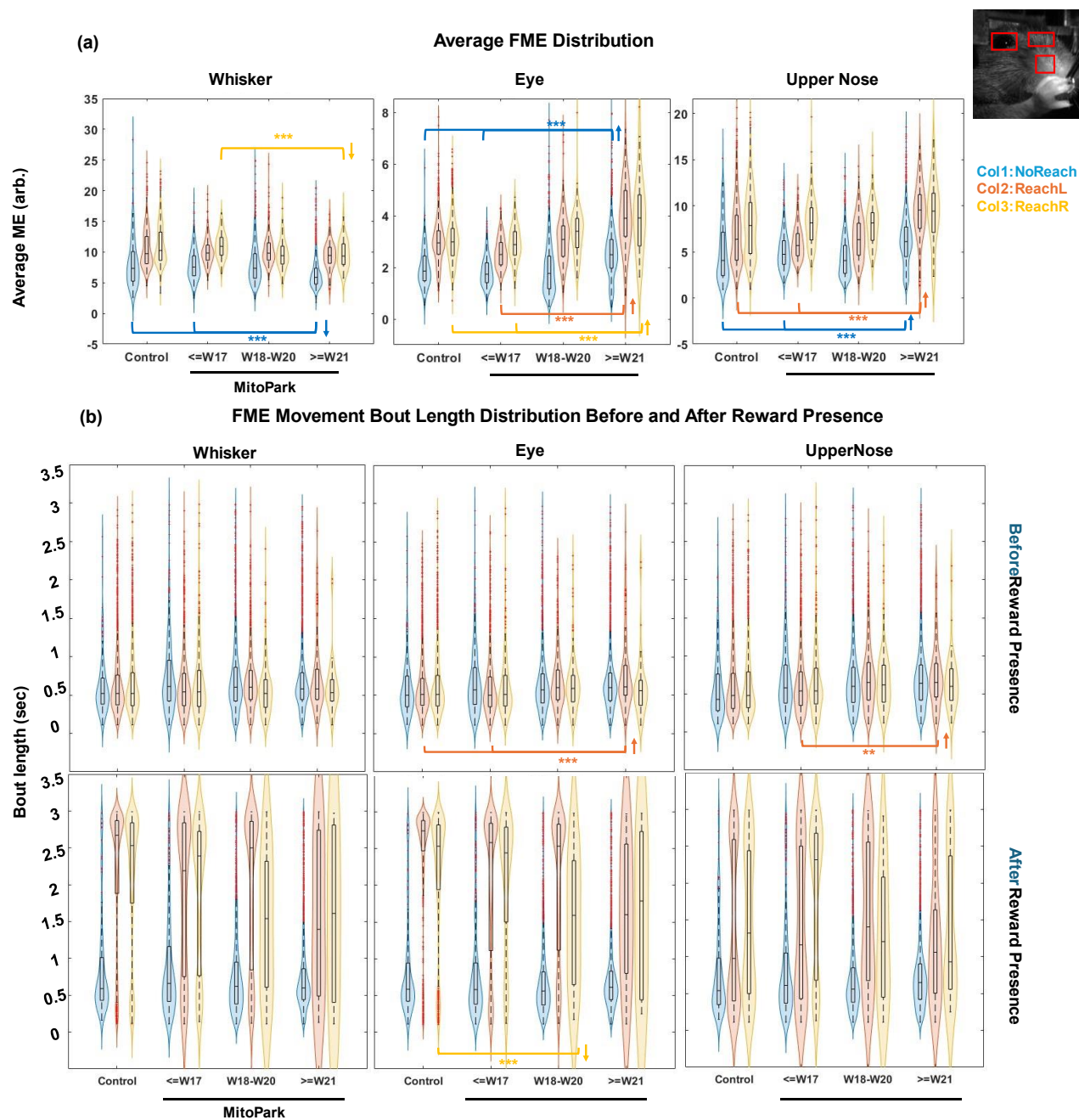
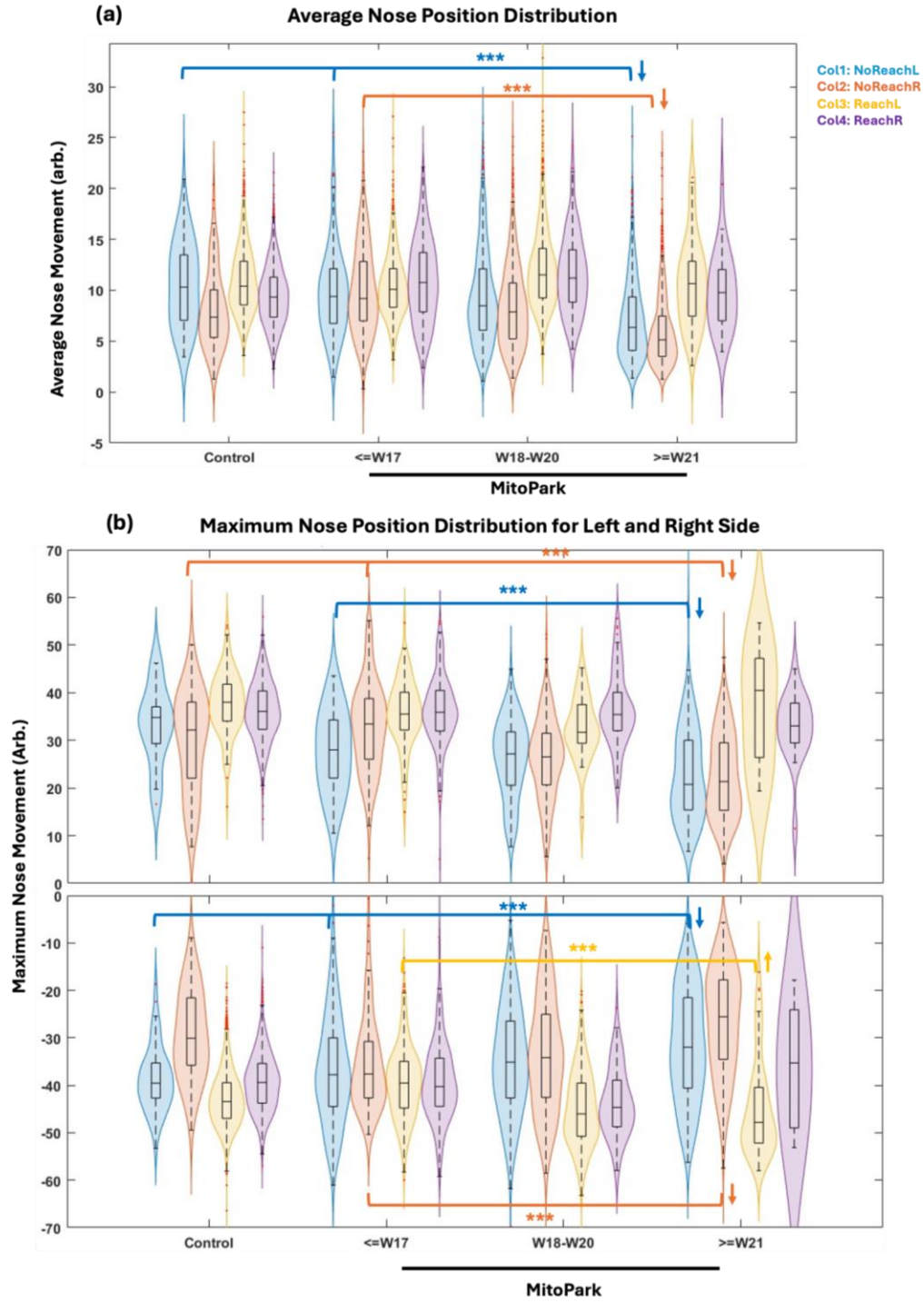


Fig. 12: Violin plots showing the distribution of average activity **(a)** and movement bout length **(b)** for facial motion energy (FME) traces across trial types and mouse groups. Each violin represents the kernel density estimate of the sample distribution. Statistical comparisons were conducted using U-tests, with significance indicated by asterisks (* $p < 0.05$, ** $p < 0.01$, *** $p < 0.001$) and horizontal brackets, with arrowing indicating directionality of change for the

medians comparing right-side groups to left-side groups. Bootstrapped median differences with 95% confidence intervals (CIs) are reported for comparisons between unimodal distributions, based on empirical peak separation and height thresholds. For comparisons involving advanced MitoPark mice (\geq W21), significance is only annotated when Control (CT) vs. Early-age MitoPark (\leq W17) was not significant.

Panel (a): In the whisker ROI, average FME was significantly reduced in \geq W21 MitoPark mice compared to Controls and \leq W17 mice during NoReach (CT vs. \geq W21: median diff = -1.48 CI = $[-2.27, -0.91]$, $p < 0.001$; \leq W17 vs. \geq W21: -1.31 $[-1.49, -1.10]$, $p < 0.001$) and ReachR trials (CT vs. \geq W21: -0.92 $[-2.25, 0.72]$, $p < 0.05$; \leq W17 vs. \geq W21: -1.59 $[-2.89, -0.03]$, $p < 0.001$). In contrast, FME increased with age in Eye and UpperNose ROIs across multiple trial types. For NoReach: Eye (CT vs. \geq W21: 0.64 $[0.51, 0.77]$, $p < 0.001$; \leq W17 vs. \geq W21: 0.76 $[0.65, 0.84]$, $p < 0.001$), UpperNose (\leq W17 vs. \geq W21: 1.38 $[1.08, 1.61]$, $p < 0.001$); for ReachL: Eye (\leq W17 vs. \geq W21: 1.40 $[1.10, 1.70]$, $p < 0.001$), UpperNose (\leq W17 vs. \geq W21: 3.85 $[3.03, 4.33]$, $p < 0.001$); and for ReachR: Eye (CT vs. \geq W21: 0.93 $[0.51, 1.49]$, $p < 0.001$; \leq W17 vs. \geq W21: 1.03 $[0.66, 1.57]$, $p < 0.001$).

Panel (b): Movement bout length analysis revealed a mild increase in bout length before reward during ReachL trials in \geq W21 MitoPark mice for the Eye (CT vs. \geq W21: 0.10 $[0.05, 0.17]$, $p < 0.001$; \leq W17 vs. \geq W21: 0.11 $[0.05, 0.21]$, $p < 0.001$) and UpperNose ROIs (ReachL: 0.11 $[0.04, 0.18]$, $p < 0.01$). Statistical results for post-reward UpperNose bout length were omitted due to distribution bimodality and low sample count.



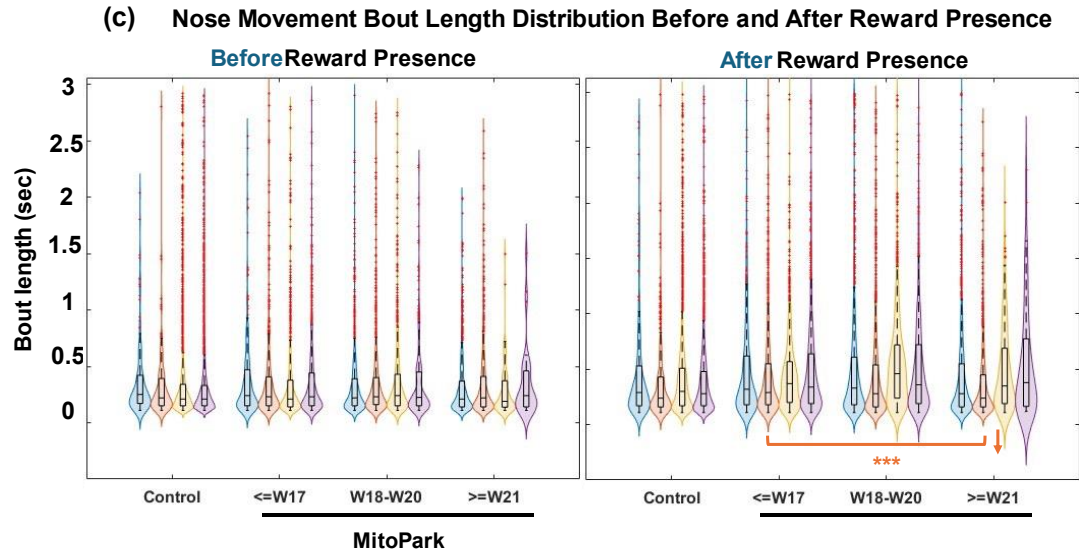


Fig. 13: Violin plots showing distributions of (a) average horizontal nose position, (b) peak nose position amplitude (top: rightward movement; bottom: leftward movement), and (c) movement bout length across mouse groups and trial types. **Panel (a):** average nose position during NoReachL was significantly lower in $\geq W21$ MitoPark mice than in Controls (-3.96 [$-5.88, -2.23$], $p < 0.001$) and $\leq W17$ mice (-3.04 [$-3.76, -2.15$], $p < 0.001$). A similar reduction was seen in NoReachR ($\leq W17$ vs. $\geq W21$: -4.07 [$-4.92, -3.36$], $p < 0.001$).

Panel (b), Top: rightward peak amplitude during NoReachR was lower in $\geq W21$ compared to both Control (-10.81 [$-13.82, -6.12$], $p < 0.001$) and $\leq W17$ mice (-12.08 [$-14.21, -9.74$], $p < 0.001$), and during NoReachL ($\geq W21$ vs. $\leq W17$: -8.27 [$-10.71, -5.35$], $p < 0.001$). **Panel (b), Bottom:** absolute leftward peak was reduced in NoReachL for $\geq W21$ vs. Control (-7.60 [$-10.11, -4.59$], $p < 0.001$) and vs. $\leq W17$ (-5.81 [$-7.86, -3.57$], $p < 0.001$), and in NoReachR ($\leq W17$ vs. $\geq W21$: -12.07 [$-14.41, -8.79$], $p < 0.001$). In contrast, ReachL trials showed increased absolute leftward amplitude in $\geq W21$ vs. $\leq W17$ (8.27 [$5.35, 10.71$], $p < 0.001$).

Panel (c): shows shorter after-reward bout lengths in \geq W21 MitoPark mice during NoReachR (-5 $[-8, -2]$, $p < 0.001$) compared to \leq W17.

Chapter 4: Discussion

The objective of this study is to characterize age-related changes in facial and nose movements of MitoPark mice during a head-fixed, bi-directional water-reaching task. As the MitoPark mice age, the loss of DA terminals in striatum and cell bodies in SN as shown in Fig. 6 and the progressive decline of reaching performance and slowed reaction time (Fig. 7) align with the DA deficiency in the nigrostriatal system and motor symptom progression timeline observed in this PD mouse model^{11,10}. Given the limited sample size of MitoPark mice ($n = 4$) and the unequal number of trials contributed by each mouse (Supp. Table 1 & 2), pooled distributions may not be representative of individual variability. To address this limitation, we incorporated mouse-level weekly averages when discussing pooled results to better account for individual variability.

4.1 Facial movement alterations in MitoPark mice

Facial motion energy (FME) effectively captured subtle facial movements such as blinking and whisking during reward-reaching behavior, and distinct FME patterns emerged across trial types and over time (Fig. 8 & 9). Within-group comparisons show that No Response trials generally had lower FME than Reach trials (Fig. 12a). Cross-age analyses revealed that average motion in the Whisker region declined for all trial types after 21 weeks of age, a trend observed in all four MitoPark mice (Supp. Fig. 1b), although less pronounced in mouse SE233 and SE240, which showed onset only after week 20. This decrease is consistent with clinical features of hypomimia, such as reduced spontaneous facial activity and diminished facial muscle mobility¹⁸.

In contrast, motion energy in the Eye and Upper Nose regions increased with age in MitoPark mice (Fig. 12a), driven primarily by mouse IM136 and IM138 (Supp. Fig. 1a). While such increases may reflect more frequent blinking or squinting, this finding contradicts clinical observations in Parkinson's disease (PD) patients, where hypomimia is typically associated with reduced blink rate¹⁹, linked to dopaminergic dysfunction in the central nervous system²⁰. One explanation for this discrepancy may be increased stress from head fixation²¹ or frustration from impaired reaching performance. Notably, MitoPark mice with high eye motion in later weeks also showed more closed eyelids compared to controls and early sessions, which may indicate emerging eyelid abnormalities²².

For movement bout analysis using the pooled data, we found a slight increase in movement bout length both before and after reward delivery. However, this measurement was highly variable across individual mice and weeks (Supp. Fig. 2). Instead, we quantified the number of movement bouts occurring within the reward response time window (Supp. Fig. 2). For both ROIs, the number of movement bouts exhibited an increasing trend across all trial types, both before and after reward delivery, as the MitoPark mice aged. An example trial with FME traces showing high occurrences of movement bouts is provided in Supp. Fig. 3. An increased number of facial movement bouts—particularly during the pre-reward period—may reflect difficulty in maintaining sustained or smooth facial motion. This pattern could be indicative of facial tremor, which manifests as involuntary, rhythmic shaking and was visibly detectable in some of the video recordings during baseline periods²³. However, additional evidence from a larger cohort is needed to support this observation, as facial tremor in PD is commonly observed at disease onset and it is still uncertain the association between facial tremor and PD progression²⁴.

4.2 Nose movement alternations evidenced by overall amplitude change

Unlike FME, nose movement traces showed less distinction between No Response and Reach trials; however, these measurements revealed more unique lateral movement patterns in response to left vs. right sensory cues. For instance, some mice developed a strategy for lateral nose movement as they mastered the reaching task, initiating movement toward a preferred side prior to water delivery and then correcting their trajectory toward the actual reward location (Fig. 10 & 11), where this bias might be shaped by asymmetrical spout placement in the setup during the training period. This pattern suggests that some animals may rely on more than just chemosensation to detect the presence of water droplets²⁵. Additionally, they may engage in a preparatory or exploratory phase before reward delivery, reflecting how animals integrate both experience-shaped habits from training and real-time sensory information into their motor planning and execution.

Overall, horizontal nose movement amplitude decreased with age in MitoPark mice, a trend confirmed by both pooled and individual analyses (Fig. 13a, Supp. Fig. 3, and Supp. Fig 4 for a sample trial with nose movement traces). This reduction may reflect impaired motor control of the nose, diminished motivation, or olfactory dysfunction. Olfactory deficits are seen in both PD patients and MitoPark mice: in human, α -Synuclein-related pathology is thought to present in the olfactory bulb—the first olfactory processing station containing dopaminergic neurons—in 90% of early-stage PD cases, affecting patients' ability to detect, identify, and discriminate odors^{9,26}. In MitoPark mice, studies have similarly reported impaired odor detection, along with a reduction in dopaminergic neurons in the olfactory bulb associated with mitochondrial dysfunction²⁷. Additionally, we observed a slight reduction in the frequency of nose movement bouts both before and after reward delivery as the MitoPark mice aged (Supp. Fig. 3). This may

reflect a decline in sniffing behavior, potentially linked to olfactory impairments, consistent with observations of reduced sniffing in PD patients^{26,28}.

This study contributes to establishing a more complete non-motor symptom profile of the MitoPark mouse model by revealing age-related changes in facial and nose movements during a goal-directed task. While MitoPark mice are widely used for studying locomotor decline, our analysis highlights subtle yet progressive impairments in spontaneous facial movement, movement consistency, and olfactory deficits—features often overlooked in traditional locomotion assessments. Moreover, the FME and nose-tracking framework developed here provides a scalable approach for future studies aiming to link specific circuit manipulations or therapeutic interventions to understand Parkinsonism symptoms in rodent models.

4.3 Limitation and future direction

As noted earlier, the small sample size and uneven trial contributions from each mouse limit the generalizability of our conclusions. Although lighting variations were corrected for in FME calculations, recording resolution for certain ROI remain potential confounders. Moreover, stress or discomfort from head fixation may influence facial expression, and these effects may be amplified in MitoPark mice as their condition deteriorates²⁹.

Future work could expand the analysis by incorporating pupil diameter dynamics and detailed eye movement recordings using a dedicated camera directed at the eye. Slower pupil responses and increased constriction latency are linked to autonomic dysfunction, a common pathological feature in PD³⁰. Additionally, given the availability of forelimb reaching data, tracking forelimb movement could help assess coordination between reaching behavior and facial movements, especially when comparing MitoPark and control mice. Time-series classification models, such

as recurrent neural networks (RNNs), could also be applied to FME or nose displacement traces to identify critical timepoints that predict trial outcomes or genotypes. To further validate and generalize these findings, future experiments could include behavioral assays in freely moving mice, where spontaneous facial expressions and motor activity are less constrained by stress or head-fixation.

References

- (1) Poewe, W.; Seppi, K.; Tanner, C. M.; Halliday, G. M.; Brundin, P.; Volkmann, J.; Schrag, A.-E.; Lang, A. E. Parkinson Disease. *Nat Rev Dis Primers* **2017**, *3* (1), 17013.
<https://doi.org/10.1038/nrdp.2017.13>.
- (2) Bologna, M.; Fabbrini, G.; Marsili, L.; Defazio, G.; Thompson, P. D.; Berardelli, A. Facial Bradykinesia. *J Neurol Neurosurg Psychiatry* **2013**, *84* (6), 681–685.
<https://doi.org/10.1136/jnnp-2012-303993>.
- (3) Gunnery, S. D.; Habermann, B.; Saint-Hilaire, M.; Thomas, C. A.; Tickle-Degnen, L. The Relationship between the Experience of Hypomimia and Social Wellbeing in People with Parkinson's Disease and Their Care Partners. *Journal of Parkinson's Disease* **2016**, *6* (3), 625–630. <https://doi.org/10.3233/JPD-160782>.
- (4) Pong, M.; Horn, K. M.; Gibson, A. R. Pathways for Control of Face and Neck Musculature by the Basal Ganglia and Cerebellum. *Brain Research Reviews* **2008**, *58* (2), 249–264.
<https://doi.org/10.1016/j.brainresrev.2007.11.006>.
- (5) Schneider, J. S.; Diamond, S. G.; Markham, C. H. Deficits in Orofacial Sensorimotor Function in Parkinson's Disease. *Annals of Neurology* **1986**, *19* (3), 275–282.
<https://doi.org/10.1002/ana.410190309>.
- (6) Sobel, N.; Thomason, M. E.; Stappen, I.; Tanner, C. M.; Tetrud, J. W.; Bower, J. M.; Sullivan, E. V.; Gabrieli, J. D. E. An Impairment in Sniffing Contributes to the Olfactory Impairment in Parkinson's Disease. *Proc. Natl. Acad. Sci. U.S.A.* **2001**, *98* (7), 4154–4159.
<https://doi.org/10.1073/pnas.071061598>.
- (7) Johnson, M. E.; Bergkvist, L.; Mercado, G.; Stetzk, L.; Meyerdirk, L.; Wolfrum, E.; Madaj, Z.; Brundin, P.; Wesson, D. W. Deficits in Olfactory Sensitivity in a Mouse Model of

- Parkinson's Disease Revealed by Plethysmography of Odor-Evoked Sniffing. *Sci Rep* **2020**, *10* (1), 9242. <https://doi.org/10.1038/s41598-020-66201-8>.
- (8) Postuma, R. B.; Berg, D.; Stern, M.; Poewe, W.; Olanow, C. W.; Oertel, W.; Obeso, J.; Marek, K.; Litvan, I.; Lang, A. E.; Halliday, G.; Goetz, C. G.; Gasser, T.; Dubois, B.; Chan, P.; Bloem, B. R.; Adler, C. H.; Deuschl, G. MDS Clinical Diagnostic Criteria for Parkinson's Disease. *Movement Disorders* **2015**, *30* (12), 1591–1601. <https://doi.org/10.1002/mds.26424>.
- (9) Fullard, M. E.; Morley, J. F.; Duda, J. E. Olfactory Dysfunction as an Early Biomarker in Parkinson's Disease. *Neurosci. Bull.* **2017**, *33* (5), 515–525. <https://doi.org/10.1007/s12264-017-0170-x>.
- (10) Ekstrand, M. I.; Terzioglu, M.; Galter, D.; Zhu, S.; Hofstetter, C.; Lindqvist, E.; Thams, S.; Bergstrand, A.; Hansson, F. S.; Trifunovic, A.; Hoffer, B.; Cullheim, S.; Mohammed, A. H.; Olson, L.; Larsson, N.-G. Progressive Parkinsonism in Mice with Respiratory-Chain-Deficient Dopamine Neurons. *Proc. Natl. Acad. Sci. U.S.A.* **2007**, *104* (4), 1325–1330. <https://doi.org/10.1073/pnas.0605208103>.
- (11) Ekstrand, M. I.; Galter, D. The MitoPark Mouse – An Animal Model of Parkinson's Disease with Impaired Respiratory Chain Function in Dopamine Neurons. *Parkinsonism & Related Disorders* **2009**, *15*, S185–S188. [https://doi.org/10.1016/S1353-8020\(09\)70811-9](https://doi.org/10.1016/S1353-8020(09)70811-9).
- (12) Langley, M. R.; Ghaisas, S.; Palanisamy, B. N.; Ay, M.; Jin, H.; Anantharam, V.; Kanthasamy, A.; Kanthasamy, A. G. Characterization of Nonmotor Behavioral Impairments and Their Neurochemical Mechanisms in the MitoPark Mouse Model of Progressive Neurodegeneration in Parkinson's Disease. *Experimental Neurology* **2021**, *341*, 113716. <https://doi.org/10.1016/j.expneurol.2021.113716>.

- (13) Waddington, J. L.; O’Sullivan, G. J.; Tomiyama, K. Regulation Of Orofacial Movement: Dopamine Receptor Mechanisms And Mutant Models. In *International Review of Neurobiology*; Elsevier, 2011; Vol. 97, pp 39–60. <https://doi.org/10.1016/B978-0-12-385198-7.00002-3>.
- (14) Nascimento, G. C.; Jacob, G.; Milan, B. A.; Leal-Luiz, G.; Malzone, B. L.; Vivanco-Estela, A. N.; Escobar-Espinal, D.; Dias, F. J.; Del-Bel, E. Brainstem Modulates Parkinsonism-Induced Orofacial Sensorimotor Dysfunctions. *International Journal of Molecular Sciences* **2023**, *24* (15), 12270. <https://doi.org/10.3390/ijms241512270>.
- (15) Tomiyama, K.; McNamara, F. N.; Clifford, J. J.; Kinsella, A.; Koshikawa, N.; Waddington, J. L. Topographical Assessment and Pharmacological Characterization of Orofacial Movements in Mice: Dopamine D1-like vs. D2-like Receptor Regulation. *European Journal of Pharmacology* **2001**, *418* (1–2), 47–54. [https://doi.org/10.1016/S0014-2999\(01\)00908-6](https://doi.org/10.1016/S0014-2999(01)00908-6).
- (16) Meyer-Baese, L.; Morrissette, A. E.; Wang, Y.; Le Chatelier, B.; Borden, P. Y.; Keilholz, S. D.; Stanley, G. B.; Jaeger, D. Cortical Networks Relating to Arousal Are Differentially Coupled to Neural Activity and Hemodynamics. *J. Neurosci.* **2024**, *44* (25), e0298232024. <https://doi.org/10.1523/JNEUROSCI.0298-23.2024>.
- (17) Mathis, A.; Mamidanna, P.; Cury, K. M.; Abe, T.; Murthy, V. N.; Mathis, M. W.; Bethge, M. DeepLabCut: Markerless Pose Estimation of User-Defined Body Parts with Deep Learning. *Nat Neurosci* **2018**, *21* (9), 1281–1289. <https://doi.org/10.1038/s41593-018-0209-y>.
- (18) Bianchini, E.; Rinaldi, D.; Alborghetti, M.; Simonelli, M.; D’Audino, F.; Onelli, C.; Pegolo, E.; Pontieri, F. E. The Story behind the Mask: A Narrative Review on Hypomimia in

Parkinson's Disease. *Brain Sciences* **2024**, *14* (1), 109.

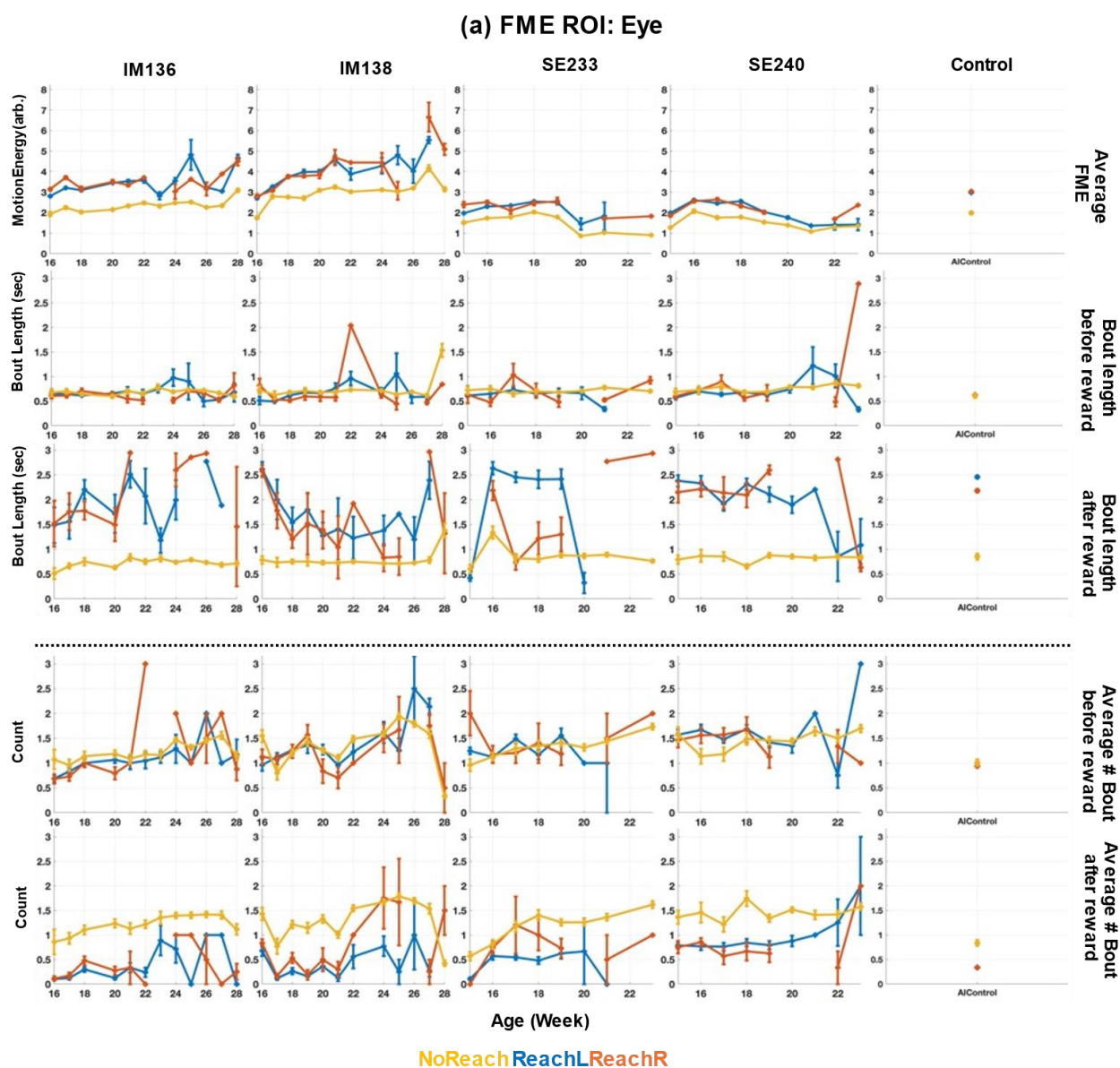
<https://doi.org/10.3390/brainsci14010109>.

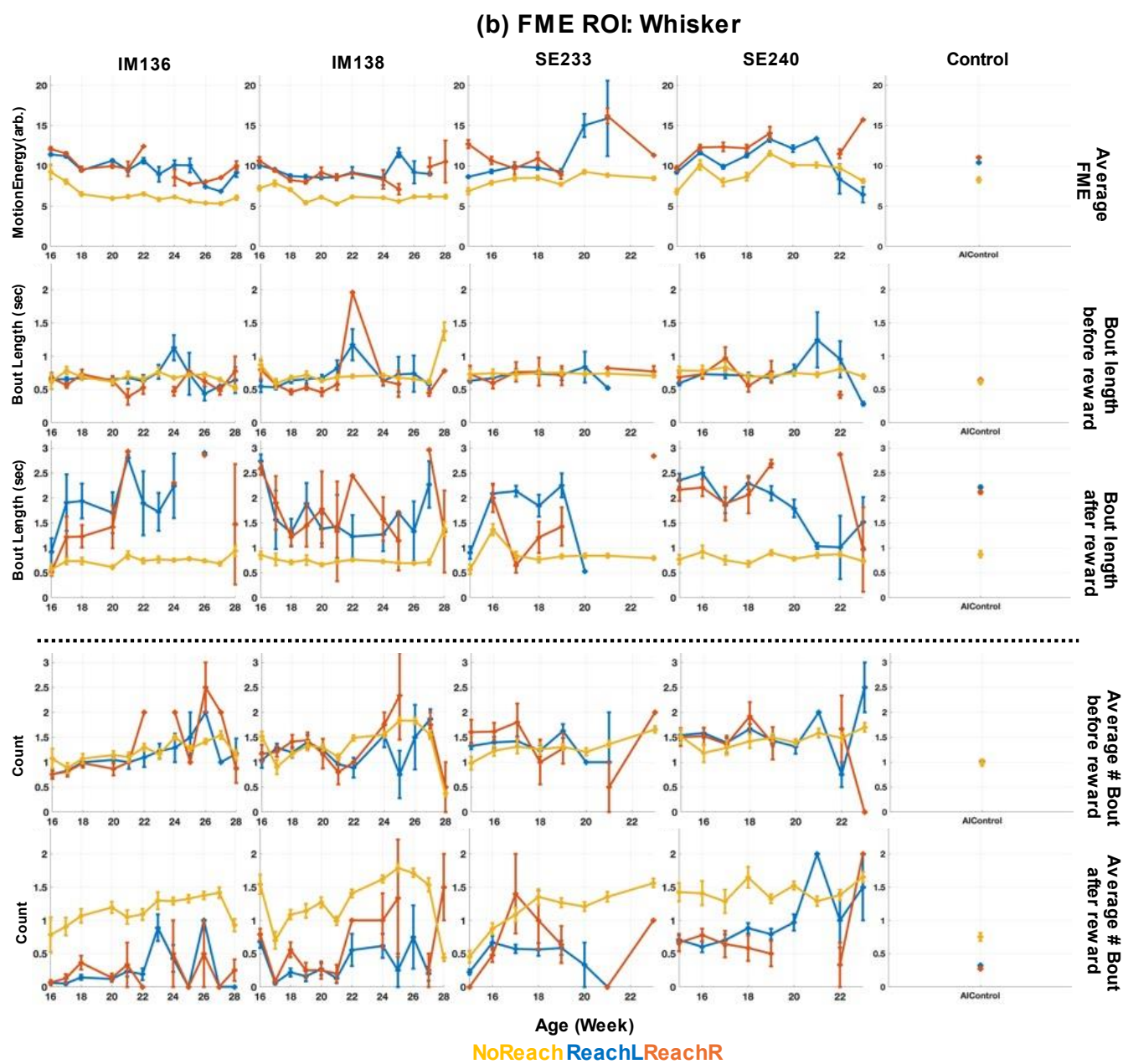
- (19) Deuschl, G.; Goddemeier, C. Spontaneous and Reflex Activity of Facial Muscles in Dystonia, Parkinson's Disease, and in Normal Subjects. *Journal of Neurology, Neurosurgery & Psychiatry* **1998**, *64* (3), 320–324. <https://doi.org/10.1136/jnnp.64.3.320>.
- (20) Karson, C. N. SPONTANEOUS EYE-BLINK RATES AND DOPAMINERGIC SYSTEMS. *Brain* **1983**, *106* (3), 643–653. <https://doi.org/10.1093/brain/106.3.643>.
- (21) Juczewski, K.; Koussa, J. A.; Kesner, A. J.; Lee, J. O.; Lovinger, D. M. Stress and Behavioral Correlates in the Head-Fixed Method: Stress Measurements, Habituation Dynamics, Locomotion, and Motor-Skill Learning in Mice. *Sci Rep* **2020**, *10* (1), 12245. <https://doi.org/10.1038/s41598-020-69132-6>.
- (22) Armstrong, R. A. Oculo-Visual Dysfunction in Parkinson's Disease. *Journal of Parkinson's Disease* **2015**, *5* (4), 715–726. <https://doi.org/10.3233/JPD-150686>.
- (23) Ou, R.; Wei, Q.; Hou, Y.; Zhang, L.; Liu, K.; Lin, J.; Jiang, Z.; Zhao, B.; Cao, B.; Shang, H. Facial Tremor in Patients with Parkinson's Disease: Prevalence, Determinants and Impacts on Disease Progression. *BMC Neurol* **2021**, *21* (1), 86. <https://doi.org/10.1186/s12883-021-02105-y>.
- (24) Rossi, M.; Wilken, M.; Morisset, P.; Fariña, S.; Cerquetti, D.; Merello, M. Facial Tremors in Patients with and without Parkinsonism. *Neurol Sci* **2016**, *37* (12), 1999–2002. <https://doi.org/10.1007/s10072-016-2683-x>.
- (25) Galiñanes, G. L.; Bonardi, C.; Huber, D. Directional Reaching for Water as a Cortex-Dependent Behavioral Framework for Mice. *Cell Reports* **2018**, *22* (10), 2767–2783. <https://doi.org/10.1016/j.celrep.2018.02.042>.

- (26) Doty, R. L. Olfactory Dysfunction in Parkinson Disease. *Nat Rev Neurol* **2012**, *8* (6), 329–339. <https://doi.org/10.1038/nrneurol.2012.80>.
- (27) Paß, T.; Aßfalg, M.; Tolve, M.; Blaess, S.; Rothermel, M.; Wiesner, R. J.; Ricke, K. M. The Impact of Mitochondrial Dysfunction on Dopaminergic Neurons in the Olfactory Bulb and Odor Detection. *Mol Neurobiol* **2020**, *57* (9), 3646–3657. <https://doi.org/10.1007/s12035-020-01947-w>.
- (28) Hawkes, C. Olfaction in Neurodegenerative Disorder. *Movement Disorders* **2003**, *18* (4), 364–372. <https://doi.org/10.1002/mds.10379>.
- (29) Domínguez-Oliva, A.; Mota-Rojas, D.; Hernández-Avalos, I.; Mora-Medina, P.; Olmos-Hernández, A.; Verduzco-Mendoza, A.; Casas-Alvarado, A.; Whittaker, A. L. The Neurobiology of Pain and Facial Movements in Rodents: Clinical Applications and Current Research. *Front. Vet. Sci.* **2022**, *9*, 1016720. <https://doi.org/10.3389/fvets.2022.1016720>.
- (30) Micieli, G.; Tosi, P.; Marcheselli, S.; Cavallini, A. Autonomic Dysfunction in Parkinson's Disease.

Supplementary figures

Supp Fig 1: Average values per week for all FME-derived statistics in two ROIs—Eye (a) and Whisker (b)—for each individual MitoPark mouse. Figures above the dashed lines are weekly mean values \pm SEM for average FME per trial, as well as movement bout length before and after reward. Figures below the dashed lines are the average number of movement bouts before and after reward. Note the imbalanced trial contributions across mice: SE233 and SE240 generally contributed fewer sessions, especially in the \geq W21 age range, compared to IM136 and IM138.

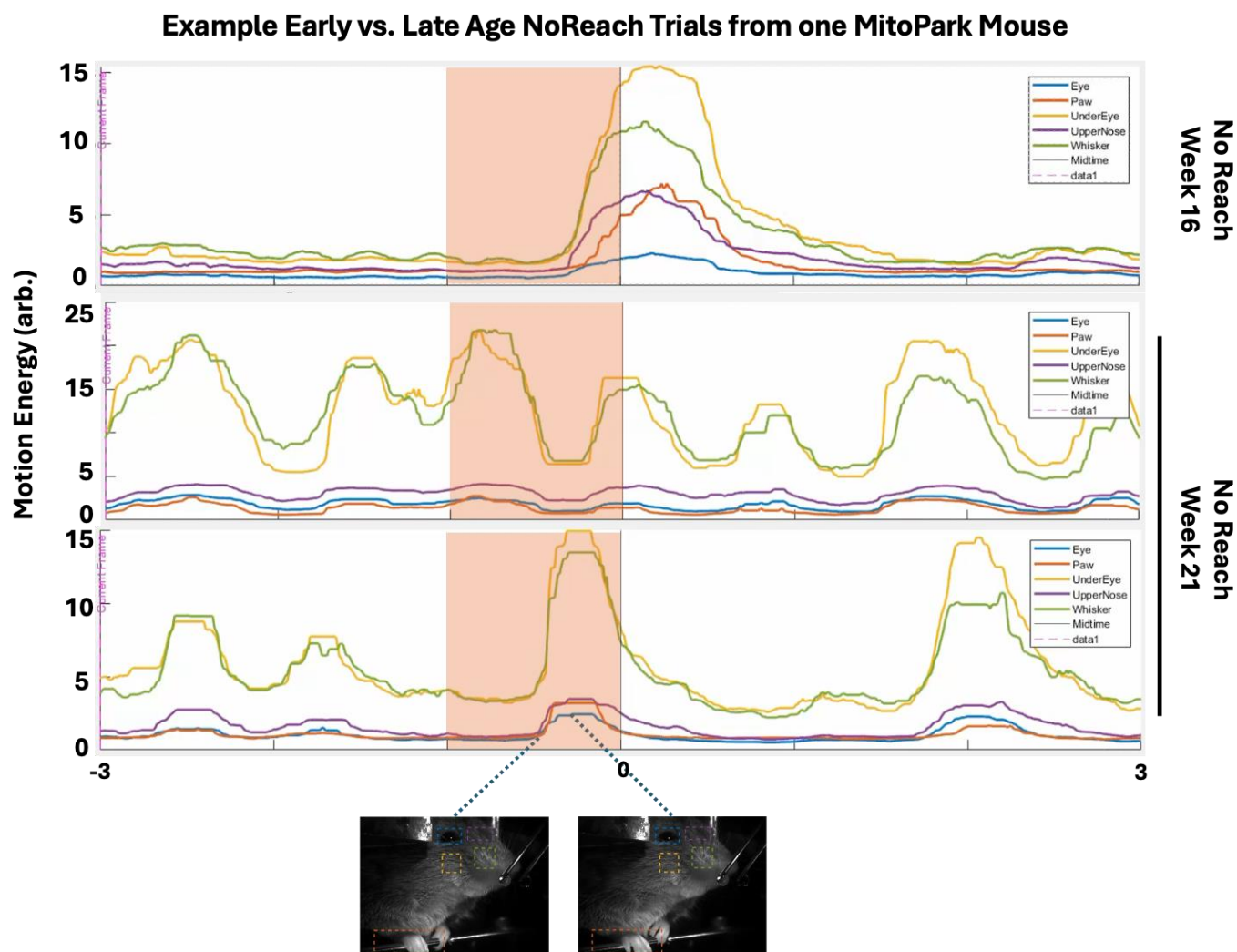




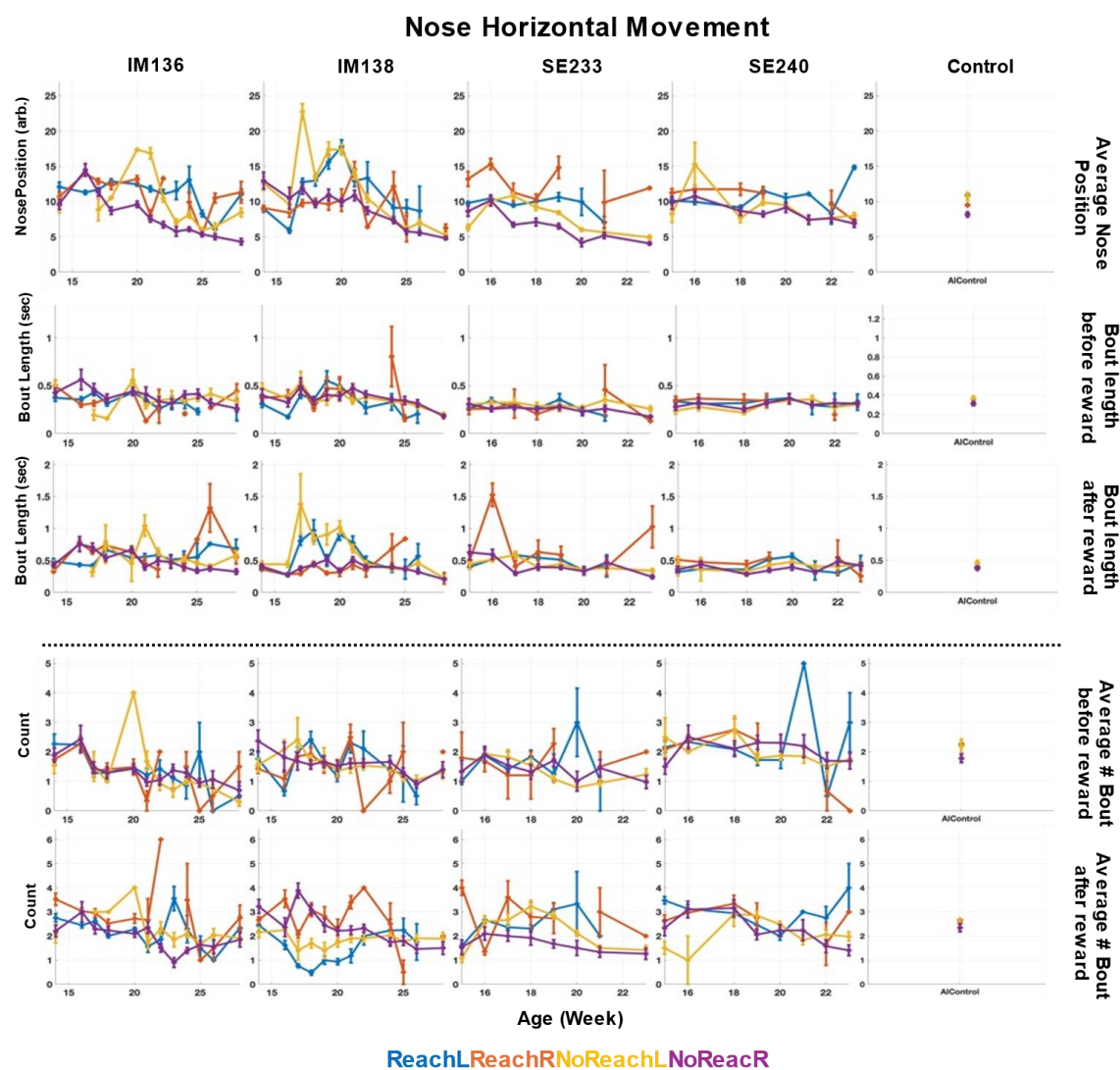
Supp. Table 1: Number of trials per trial type used in the FME analysis for each MitoPark mouse.

	MitoPark mouse_ID			
	IM136	IM138	SE233	SE240
ReachL	455	293	387	324
ReachR	200	177	52	101
NoReach	1141	1370	915	665

Supp Fig 2: (a) Example NoReach trials from a single MitoPark mouse across early ($W \leq 17$) and late ($W \geq 21$) sessions, illustrating a higher occurrences of short facial movement bouts in the late session.



Supp. Fig 3: Average values \pm SEM per week for all nose movement statistics calculated for each individual MitoPark mouse and pooled controls.



Supp. Table 2: Number of trials per trial type used in the nose movement analysis for each MitoPark mouse.

	MitoPark mouse_ID			
	IM136	IM138	SE233	SE240
ReachL	491	320	400	270
ReachR	243	278	52	87
NoReachL	375	696	582	395
NoReachR	628	676	349	2442

Supp Fig 4: Example NoReach trials from a MitoPark mouse comparing early and advanced-age sessions, showing reduced nose movement with age.

